ENVIRONMENTAL RESEARCH
LETTERS

LETTER • OPEN ACCESS

Dynamic sea-level changes and potential implications for storm surges in the UK: a storylines perspective

To cite this article: Claire E Bulgin *et al* 2023 *Environ. Res. Lett.* **18** 044033

ENVIRONMENTAL RESEARCH
LETTERS

LETTER

Dynamic sea-level changes and potential implications for storm surges in the UK: a storylines perspective

Claire E Bulgin[1,2,*], **Jennifer V Mecking**[3], **Ben J Harvey**[1,4], **Svetlana Jevrejeva**[5], **Niall F McCarroll**[1,2], **Christopher J Merchant**[1,2] **and Bablu Sinha**[3]

[1] Department of Meteorology, University of Reading, Reading, United Kingdom
[2] National Centre for Earth Observation, University of Reading, Reading, United Kingdom
[3] Marine Systems Modelling, National Oceanography Centre, Southampton, United Kingdom
[4] National Centre for Atmospheric Science, University of Reading, Reading, United Kingdom
[5] Marine Systems Modelling, National Oceanography Centre, Liverpool, United Kingdom
[*] Author to whom any correspondence should be addressed.

E-mail: c.e.bulgin@reading.ac.uk

Keywords: dynamic sea-level, storm surges, climate change, storylines

Supplementary material for this article is available online

OPEN ACCESS

RECEIVED
10 August 2022

REVISED
13 January 2023

ACCEPTED FOR PUBLICATION
23 March 2023

PUBLISHED
11 April 2023

Abstract

Global sea-level rise caused by a warming climate increases flood risk from storm surge events for those who live in coastal and low-lying areas. Estimates of global thermosteric sea-level rises are well constrained by model projections, but local variability in dynamic sea-level arising from seasonal and interannual changes is less well characterised. In this paper we use satellite altimetry observations coupled with CMIP6 model projections to understand drivers of change in dynamic sea-level over the UK shelf seas. We find a northward shift in the atmospheric jet stream and a weakening of the Atlantic meridional overturning circulation to be the key drivers of local dynamic sea-level variability. Using a storyline approach to constrain climate system responses to changes in atmospheric greenhouse gas concentrations, we find that dynamic sea-level is predicted to rise between 15–39 cm by 2080–2099 along the east coast of England (ECE). Under a worst-case scenario, assuming maximum variability as seen in the CMIP6 projections, ECE dynamic sea-level rise could reach 58 cm by 2100. We illustrate the impact of this dynamic sea-level rise in addition to non-dynamic components on the risks posed by storm surge events in ECE using an idealised example. If a storm surge event of the magnitude of the one experienced in ECE on the 5th of December 2013 was to occur in 2100, an additional 1414 km^2 of land would potentially be affected in our worst-case idealised example, 22.4% of which can be attributed to dynamic sea-level rise.

1. Introduction

Global sea-level rise is one of the impacts most confidently attributable to anthropogenic global warming and is an integral measure of heating of the climate system [1]. The Intergovernmental Panel on Climate Change (IPCC) AR6 WG1 Summary for Policymakers states that there is high confidence that the rate of mean global sea-level rise increased from 1.3 ± 0.8 mm yr^{-1} during the period 1901–1971 to 3.7 ± 0.5 mm yr^{-1} during the period 2006–2018 [2]. Human influences are very likely to be the main driver of this acceleration [2]. The accumulated mean sea-level rise is estimated to be 0.2 ± 0.05 m today relative to preindustrial times [1]. Confidence in attributing causes of global sea-level increase is based on the well-understood mechanisms of sea-level change at global spatial scales. The two largest causes are thermosteric expansion with increasing ocean heat content and change in the total mass of the ocean due to ice mass loss from glaciers and ice sheets in Greenland and Antarctica [1, 3].

Sea level rise is non-uniform around the globe and strongly influenced by a variety of processes, including direct atmospheric forcing (inverse barometer (IB) effect); ocean dynamical processes which may be forced dynamically (wind) or thermodynamically (surface buoyancy flux); hydrological (e.g. sediment redistribution, freshwater input) and geological processes (e.g. isostatic rebound); and human activities

(e.g. land reclamation, water storage in artificial reservoirs and groundwater extraction) [1]. Hence, understanding of regional sea-level rise is complex, as well as being crucial to the socioeconomic well-being of the rapidly growing proportion of the human population that inhabits the world's coastlines [2]. Projected global mean sea-level rise by 2100 will alter the height and frequency of extreme water events [1, 4], thus shifting flood and inundation risks for low-lying areas [4, 5].

Although current climate models (e.g. Coupled Model Intercomparison Project Phase 6 (CMIP6) [6]) often lack the horizontal and vertical resolution to fully resolve small-scale processes in shallow areas [3], they all have a basic representation of shelf-sea processes and hence can provide a useful indicator of regional future sea-level changes. However, uncertainties can be large, with projections suffering from uncertainties that arise from a lack of knowledge or understanding of the modelled processes and uncertainties that arise from random or chaotic parts of the modelled system [6]. In addition, mean sea-level projections are often focussed on long-term averages (from multi-model means) over extended periods. In most coastal locations observations reveal the presence of strong seasonal and interannual variability [7, 8], and the impacts of changes in such variability are currently not accounted for in projections. In this context, the multi-model mean dynamic response (often used as a 'best estimate' for future predictions) arguably does not provide an adequate basis for policy decisions.

A richer approach to understanding future changes is the use of storylines, which are 'physically self-consistent plausible future events or pathways' [9]. The storylines approach can improve the evidence base by providing plausible outcomes conditional on particular actions (such as humanity limiting the amount of carbon dioxide emitted to the atmosphere), and/or conditional on uncertain aspects of the climate-system response (such as whether a major perturbation in North Atlantic circulation does or does not occur). Storylines can be informed both by long-term historical observations of essential climate variables and by model projections.

Impact and risk assessment, adaptation policies and long-term decision making in coastal areas are crucially informed by projected changes in local relative mean-sea-level (MSL) and extreme sea-level events [1, 10]. Recent studies suggest that extreme sea-level events associated with tropical and extratropical storm surges with a one-hundred-year return time could occur every year by the end of this century [1, 4]. Even with global warming limited to 1.5–2 K, projected mean sea-level rise in tropical areas will more than double the frequency of extreme sea-levels and increase coastal flood risk [1]. With a further mean sea-level rise of 0.15 m, the global population exposure to a 100 year coastal flood will increase by 20% [11], leading to an economic impact in coastal areas through the loss of land, infrastructure and physical capital and an increase in expenditure for coastal protection [11, 12].

In this paper, we focus on dynamic sea-level changes over the shelf seas surrounding the British Isles. This area is of particular interest in the context of understanding future changes in the North Atlantic circulation (both oceanic and atmospheric), air-sea interactions [13, 14] and the propagation of such open-ocean changes into neighbouring shallow shelf-sea waters. Rising sea-levels around the British Isles have implications for the frequency and magnitude of storm surges with corresponding impacts on the economic and human costs of flooding events [10, 15].

The paper is structured as follows. Sea-level anomalies in the recent satellite era are characterised in section 2. Section 3 introduces the CMIP6 models, comparing simulations with satellite observations over the historical period and presenting projections for 2080–2099. Section 4 introduces four different dynamic storylines for future dynamic sea-level change and describes the worst-case scenarios as projected by the CMIP6 models. It also includes an idealised example of an event storyline to illustrate the combined impact of future mean sea-level rise, plus changes in seasonal and interannual dynamic sea-level, with a storm surge event similar to that of 5 December 2013 occurring in 2100. Section 5 is a discussion and conclusion.

2. Characterising sea-level anomalies from altimetry observations

Recent changes and variability in sea-level anomalies can be assessed using satellite altimeter measurements of geocentric sea-level height. We use the European space agency (ESA) climate change initiative (CCI) sea-level anomaly (SLA) product which provides monthly gridded data between 1993–2015 [16], but limit the date range used in this study to 1993–2014 for consistency with the climate modelling component (section 3). The SLA product is calculated with reference to a mean-sea-surface-height after correction for tides, sea state bias and a dynamic atmosphere correction [17]. The spatial resolution of the data is 0.25 degrees.

As stated in the introduction, regional SLA is influenced by atmospheric pressure, but a correction has already been applied to the altimetry data to remove the IB effect [17], the magnitude of which is not specified in the data distribution. We therefore estimate the magnitude of this adjustment (η^{ib}) in the monthly products, using a standard relationship between pressure and SLA, which is valid for timescales of days to weeks [18, 19]. This is calculated independently for each grid point, using

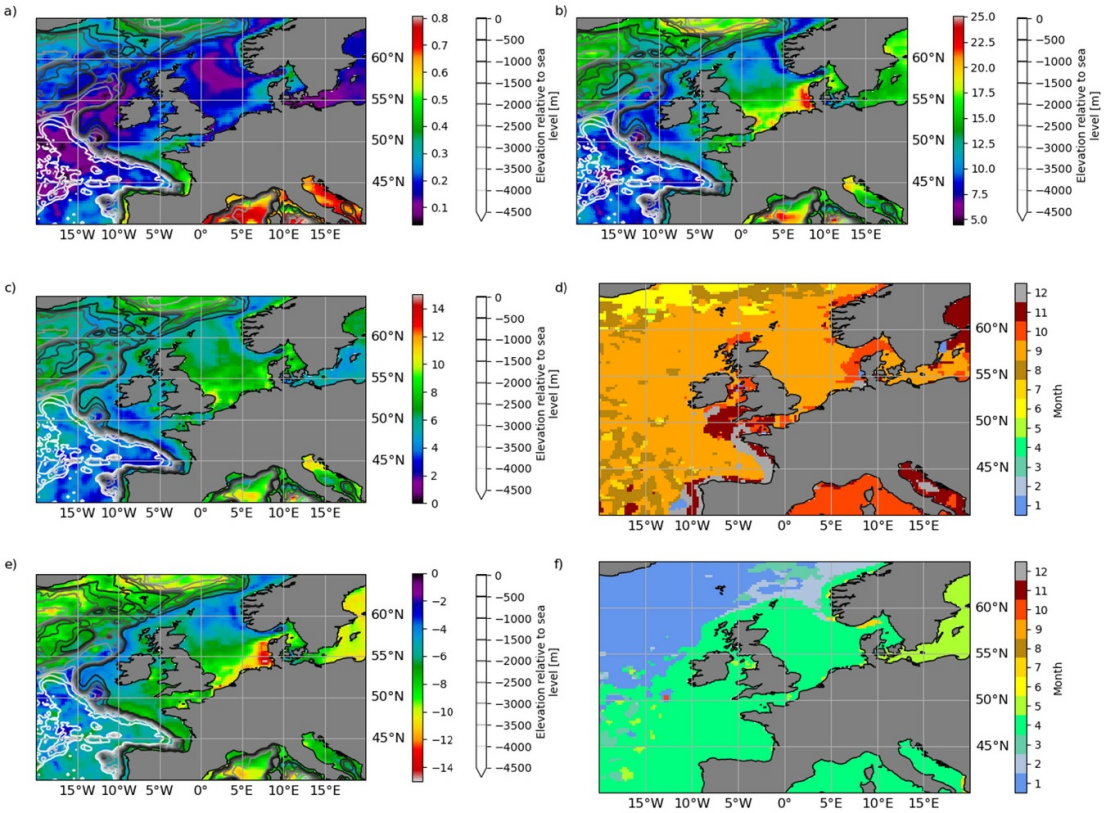

Figure 1. (a) Ratio of seasonal to total variance in ASP SLA between 1993–2014 and (b) ASP SLA range over the seasonal cycle. ASP SLA anomaly seasonal cycle maximum (c) and minimum (e), with corresponding month of maxima (d) and minima (f). Bathymetry is overplotted on panels a, b, c and e. SLA values are in units of centimetres.

ERA-5 reanalysis surface pressure data ($\boldsymbol{P_a}$) [20], with reference to a global mean surface pressure ($\overline{\boldsymbol{P}}_{\boldsymbol{a}}$) of 1013 hPa. $\boldsymbol{\rho}$ is the density of water and $\boldsymbol{g}$ the gravitational acceleration constant,

$$\eta^{ib} = -\frac{P_a - \bar{P}_a}{\rho g}. \quad (1)$$

In the remainder of section 2 we discuss the characteristics of SLA from the satellite altimetry data, where we have removed the adjustment for the IB effect, as this corresponds to the SLA measure in the CMIP models (section 3). We refer to this as the adjusted satellite product (ASP) SLA throughout the paper, and compare this to the raw ESA CCI satellite product (RSP) to characterise the influence of the atmospheric pressure on SLA. For the remainder of the paper (section 3 onwards) we use the ASP SLA data.

2.1. Seasonal variability

Figure 1 shows the seasonal characteristics of the ASP SLA data. The ratio of seasonal to total SLA variance (figure 1(a)) is typically 10%–20% across the eastern Atlantic, UK shelf seas and the North Sea. The seasonal range in SLA is <10 cm along the west coast of England, Wales and Scotland. To the east and the south of the UK, the seasonal range is larger, peaking at ∼20 cm in the south east (figure 1(b)). The largest SLA range is seen along the northern coast of Europe with a maximum along the coast of Denmark. The seasonal cycle in SLA peaks in September along the eastern coasts, across the North Sea and to the west of Ireland. Along the west coast of England, Wales and Scotland the peak SLA is seen in October in the north and November in the far south west. The seasonal minimum occurs in April for the UK shelf seas, the North Sea and around the northern European coastline. A distinct boundary is formed at the northern edge of the UK shelf, where the slope current bypasses Scotland, to the north of which, SLA peaks in January.

The ASP and RSP products can be compared with reference to figures S1 and S2. Figure S1 shows the equivalent metrics to figure 1, but for the RSP SLA. Figure S2 shows the seasonal cycle of the atmospheric pressure adjustment removed from the RSP data to generate the ASP data. This is provided for five regions around the UK, covering all of the coastline of Great Britain. These regions are defined as the west, south and east coasts of England and Wales (WCE, SCE and ECE respectively) and the west and east coasts of Scotland (WCS and ECS). The areas covered by these boxes are shown in figure 2(a).

On the western edge of the UK shelf (figure S1) more than 80% of the total monthly variance in the RSP SLA product is explained by the seasonal

Table 1. Sea-level-anomaly statistics over five regions encapsulating the UK coastline. Statistics are calculated from 22 years of ESA SLA CCI data (1993–2014) [16] and for the CMIP6 models (multi-model-means) for the same time period.

Metric	West Coast England and Wales (WCE)	South Coast England (SCE)	East Coast England (ECE)	West Coast Scotland (WCS)	East Coast Scotland (ECS)
Longitude bounds	6.5–2.5 W	6.5 W—2.0 E	2.0 W—2.5 E	8.0–4.0 W	4.0 W—0.0 E
Latitude bounds	51.25–55.0 N	49.0–51.25 N	51.25–55.5 N	55.0–59.0 N	55.5–59.0 N
RSP seasonal SLA range	14.6 cm	14.1 cm	15.6 cm	15.2 cm	14.8 cm
ASP seasonal SLA range	11.6 cm	13.0 cm	16.5 cm	11.5 cm	12.3 cm
RSP SLA interannual variability	1.3 cm	1.4 cm	1.5 cm	1.4 cm	1.3 cm
ASP SLA interannual variability	1.8 cm	1.7 cm	2.4 cm	2.2 cm	2.2 cm
Long-term trend	2.1 ± 1.8 mm yr^{-1}	2.1 ± 1.7 mm yr^{-1}	2.0 ± 2.3 mm yr^{-1}	2.5 ± 2.0 mm yr^{-1}	2.6 ± 2.0 mm yr^{-1}
CMIP6 MMM SLA seasonal range	9.7 cm	9.9 cm	15.2 cm	12.1 cm	13.3 cm
CMIP6 MMM interannual variability	2.1 cm	1.9 cm	2.9 cm	2.4 cm	2.8 cm

cycle, with a sharp contrast at the shelf boundary to just 10%–30% in deeper Atlantic waters. Closer to the UK coastline, the seasonal cycle explains 50%–60% of the total variability in the RSP data, decreasing to 30%–40% along the eastern English coastline, through the English Channel and further east across the North Sea.

The atmospheric pressure adjustment (figure S2) has a strong seasonal component due to the seasonally lower pressure in winter months compared to the summer, enhancing the seasonal signal in SLA and increasing the seasonal range. The maximum SLA occurs later (October) over much of the North Sea and western Atlantic in the RSP data. To the north of the UK the adjustment made in the RSP data is such that the SLA minimum occurs in April, similar to the shelf sea regions. The SLA range is larger in the RSP data along the western coasts of England, Wales and Scotland and the east coast of Scotland (12.5–17.5 cm).

Table 1 provides SLA statistics for the five regions around the UK. The seasonal range in the ASP SLA has a maximum in ECE (16.5 cm) and a minimum in WCS (11.5 cm). The seasonal range in the RSP data is generally larger showing small regional variations along the UK coastline with a minimum of 14.1 cm for SCE and a maximum of 15.6 cm for ECE. ECE is the only region where the seasonal range is larger in the ASP data (16.5 cm) than in the RSP data (15.6 cm).

The seasonal cycle for the ASP SLA averaged across all UK shelf-seas consists of a single oscillation per year (figure 2(b)), with a maximum in September to November and a minimum in April (figures 1(c)–(f)). The month of the maximum varies along the southern English coastline, peaking in September to the south-east and in November to the south. The region of greatest seasonal range in SLA, along the coast of Denmark, is characterised by a lower minimum in April than observed over the rest of the North Sea. The SLA seasonal cycle lags the seasonal cycle in shelf-sea sea-surface-temperature by one-to-two months (not shown). In very shallow waters, the steric component of SLA change is necessarily small, suggesting that advection and other factors such as wind are also important in translating the deep-water signal over the shelf seas.

2.2. Interannual variability

In addition to the seasonal variability, SLA varies on an interannual timescale. The interannual variability in SLA over the duration of the satellite observations is shown in table 1 for both the ASP and RSP data. This variability is calculated as the standard deviation of the annual mean SLA, after detrending and removing the seasonal cycle. The interannual variability is dampened in the RSP data, of order 1.3–1.5 cm along the UK coastline compared with 1.7–2.4 cm for the ASP data. The largest interannual variability in the ASP data is seen in ECE (2.4 cm) and the smallest in SCE (1.7 cm).

The interannual variability over the North Sea, important for SLA variability in ECE and ECS, is related primarily to the north–south and east–west

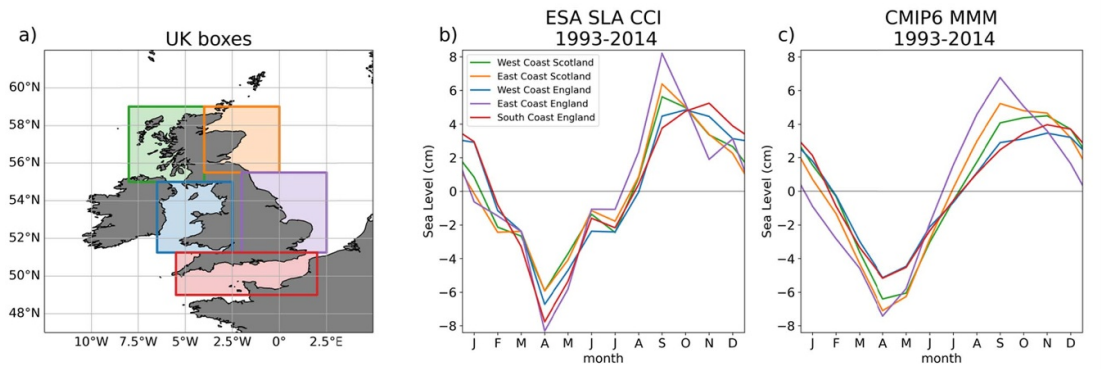

Figure 2. (a) Map showing the five boxes around the UK analysed in this study as defined in table 1: WCS (green), WCE (blue), SCE (red), ECE (purple) and ECS (orange). (b) Observed seasonal cycle in ASP SLA from the ESA CCI SLA data in the five boxes. (c) CMIP6 multi-model mean (MMM) of the seasonal cycle of dynamic sea-level in the five boxes. Month tick-marks represent the middle of each month, running from J (January) to D (December) .

wind stress (EWWS) in the region. Figures 3(a)–(d) shows local (grid-point to grid-point) correlations between the deseasonalised and detrended, ASP SLA against deseasonalised and detrended surface wind stress components for April and October (chosen as they are the minima and maxima of the SLA seasonal cycle in UK coastal waters). Monthly surface wind stress data are retrieved from the ERA5 reanalysis on a 0.25 degree grid [21], covering the same period as the SLA observations. Over the North Sea, SLA is positively correlated with the EWWS (wind blowing from the west), meaning that stronger winds from the west increase the SLA. When comparing SLA with the north–south wind stress (NSWS, wind blowing from the south) we see a weak dipole relationship in the correlation over the North Sea in April (figure 3(c)). To the north-west, SLA is uncorrelated with NSWS and to the south-east the correlation is negative.

A corresponding plot for correlations of the RSP data against EWWS and NSWS is provided in the supplementary material (figure S3). In April, the atmospheric pressure adjustment present in the RSP data is spatially consistent with the areas of correlation between SLA and both EWWS and NSWS (not shown), but of opposite sign, so it has the effect of dampening the correlations in the RSP data. In October, the atmospheric pressure adjustment is positive across the domain of interest (not shown), but weaker to the northeast of the UK resulting in a stronger correlation between the RSP SLA and EWWS over the North Sea and stronger correlation dipole between RSP SLA and NSWS over the North Sea.

This dipolar correlation pattern is related to both oceanographic and atmospheric factors. Westerly wind stress over the North Sea causes positive SLA anomalies along the Danish coast, which in turn result in a clockwise gyre corresponding to the region of negative correlation between SLA and NSWS [22]. The southerly flow of the gyre is reinforced by the southerly inflow of water from the Atlantic through the Norwegian Trench [22]. The dipole is strongest in April following increased EWWS over the winter months.

The variability of the North Atlantic atmospheric circulation is succinctly characterised by the latitude of the eddy-driven jet stream [23]. We use a jet latitude (JL) index to quantify this: the latitude of the monthly mean wind maximum at 850 hPa in the region of 0–20 W [24]. Following [25], and using the ERA5 dataset, a centroid measure of JL is computed as a meridional integral of latitude weighted by the 0–20 W mean of zonal wind speed over the region 30–70 N. Figures 3(e)–(h) compare the correlations between EWWS and NSWS with the JL index. Focussing specifically on the North Sea, we see the same relationship between JL index and wind stress as shown in panels a-d of figure 3 between SLA and wind stress. This demonstrates that the JL index captures the variability in SLA caused by both the EWWS and NSWS. Northward movement of the jet stream is strongly correlated with an increase in SLA in the ASP data over the eastern Atlantic, UK shelf seas and the North Sea (figures 3(i) and (j)).

2.3. Long-term trend

Table 1 also shows the long-term trend in the observational dataset over the 22 year period. This trend is reasonably consistent around the whole of the UK coastline (as expected) and is 2.0 $\pm$ 2.3 mm yr^{-1} (ECE) to 2.6 mm yr^{-1} $\pm$ 2.0 mm yr^{-1}. Given the large uncertainty estimates from the fitting uncertainty in table 1, this is consistent with the independent estimate from tide gauges in the State of the Climate report of 3.6 $\pm$ 1.0 mm yr^{-1} for the UK for 1993–2019 [26]. As stated in [26], UK sea level increases are non-linear, including variations on annual and decadal timescales which may also account for small differences in trends calculated over different time

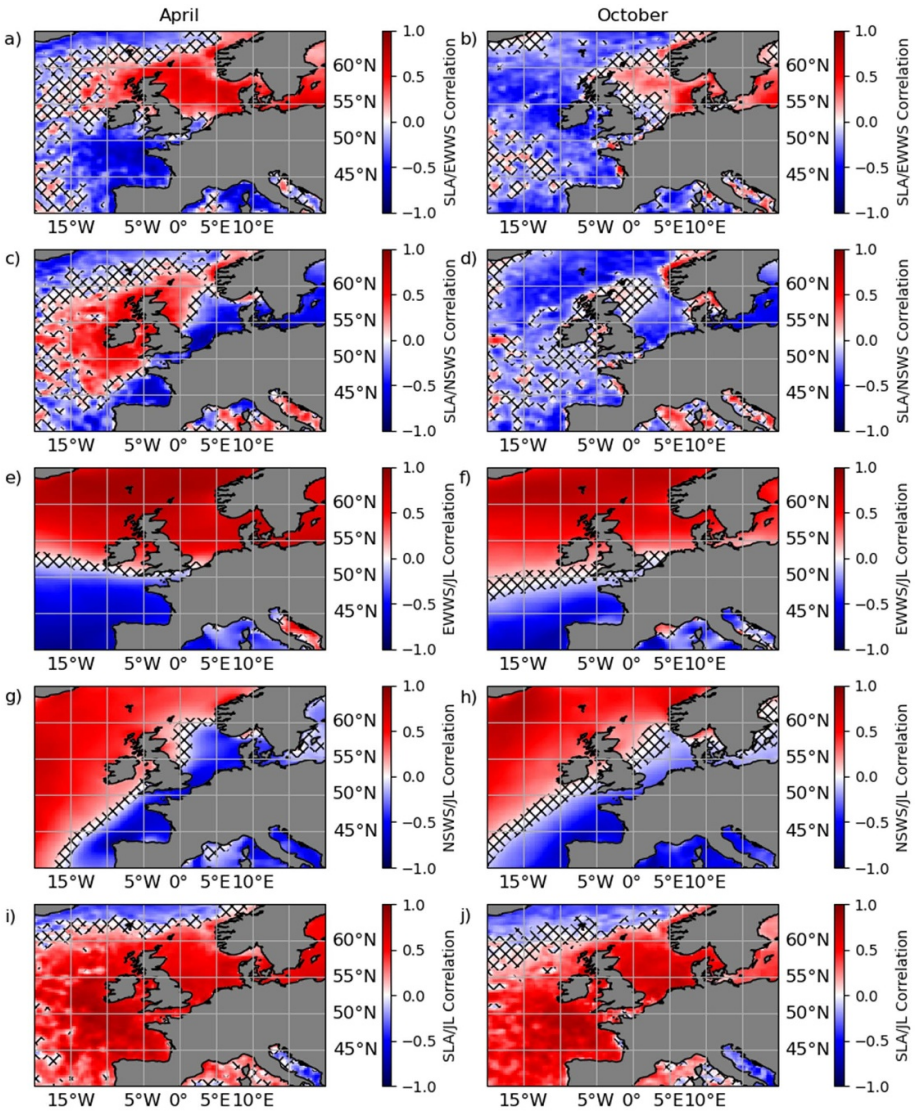

Figure 3. Main drivers of interannual variability in ASP SLA. Subplots show correlations for April (left) and October (right). Local (grid-point to grid-point) correlation of SLA with EWWS (a) and (b), local correlation of SLA with NSWS (c) and (d), correlation of local EWWS with JL index (e) and (f), correlation of local NSWS with JL index (g) and (h), and correlation of local SLA with JL index (i) and (j). Hatching shows areas where the correlation is insignificant at the 95% confidence level.

periods. The fitting uncertainty (u) given for the trend over time, represented as a linear slope, is defined in equation (2). $\sum_1^n e^2$ is the sum of the square of the residuals from the fit, n is the total number of observations and k the degrees of freedom of the fit,

$$u = \sqrt{\left(\frac{\sum_1^n e^2}{n-k}\right)}. \quad (2)$$

The magnitude of the uncertainties (table 1) is large in part because of the relatively short dataset length and the use of a linear fit which neglects the sea-level rise acceleration term [27]. This estimate also excludes the uncertainties that arise within the measurement process itself. A rigorous evaluation of the uncertainty in area-averaged SLA would require full uncertainty characterisation to enable correct uncertainty propagation [27].

3. Projected changes in sea-level anomalies

CMIP6 model data [6] can be used to constrain the plausible range of future changes in the dynamic sea-level around the UK. In this study we use 15 CMIP6 models, each with one ensemble member, chosen simply by their availability on the JASMIN super-computing facility [28]. A full list of the models and ensemble members used is provided in the Supplementary Material (table S1 [29–85]). Monthly mean dynamical sea-level ('zos') from the CMIP6 models is used in this analysis, representing dynamical sea-level changes only (excluding ocean thermal expansion

and addition of ice mass loss from ice-sheets and glaciers). No atmospheric pressure adjustment is applied to these data [86]. To match the observational dataset time period, the reference period for all comparisons with observations is 1993–2014, taken from the historical simulation for each model. We first compare simulations of dynamic sea-level for the reference period to the satellite altimetry observations to assess the degree to which the model can capture the observed SLA seasonal cycle and variability around the UK coast. Dynamic sea-level is appropriate for comparison with observational data over the shelf-seas where the long-term trend in SLA has been removed. Comparisons are made against the ASP satellite data as CMIP6 data are not adjusted for atmospheric pressure. Model data are provided at one-degree resolution, re-gridded from individual model runs that use different projections. For the purposes of comparison with the observations, data from each model are used where the grid-box-centre coordinates fall within the defined bounds of the UK boxes.

3.1. Historical seasonal cycle and dynamic sea-level variability in CMIP6

Figure 2(c) shows the SLA seasonal cycle of the CMIP6 models using the multi-model-mean (MMM) corresponding to the satellite observations (2b) for the five boxes around the UK coastline between 1993–2014. The general shape of the CMIP6 MMM seasonal cycle in SLA is similar to the observations. The September maximum in dynamic sea-level is captured by the models for ECE and ECS with later peaks in WCE and SCE. The range of the seasonal cycle in the MMM for WCE and SCE (9.7–9.9 cm) is lower than the observed SLA seasonal cycle (11.6–13.0 cm, table 1) with a maximum difference of 3.2 cm, although the observed seasonal cycle is within the spread of the models (table S2). In WCS and ECS the agreement between models and observations is closer (11.5–12.3 cm in the observations and 12.1–13.3 cm in the models). The models also capture the larger seasonal range in ECE, (16.5 cm in the observations and 15.2 cm in the CMIP6 models). Small differences between the modelled and observed seasonal cycle could be explained either by dampening of the signal in averaging the model outputs or through differences in the SLA calculation.

The interannual variability of the dynamic sea-level in each of the UK boxes is computed after removing the seasonal cycle. The maximum CMIP6 MMM variability occurs in ECE, consistent with the observations and of similar magnitude: 2.9 cm for the MMM compared to 2.4 cm for the observations. The interannual variability of the CMIP6 models across the UK boxes ranges between 1.9–2.9 cm, compared with 1.7–2.4 cm for the observations (table 1). The interannual variability also shows a positive correlation with the JL index over the North Sea (not shown), as found for the observations.

Comparison of the MMM statistics with the satellite altimetry data show that the models can reproduce the shape of the seasonal cycle and the relative differences between ECE and other UK boxes. Absolute values in the ASP data are well represented by the MMM with a tendency to underestimate the seasonal cycle around the coast of England and Wales and overestimate the seasonal cycle around the Scottish coasts. The MMM slightly overestimates the interannual variability compared to the observations, but given that the differences are small, we find the models are adequate to indicate the range and spatial variability of possible projections over the UK shelf-seas.

3.2. Future climate projections

Projections of dynamic sea-level change around the UK coastline can be obtained by comparing the historical CMIP6 simulations with simulations for a future time period under different shared socio-economic pathways (SSPs). Prior to comparison of historical and future projections, model drift ('spurious long-term changes independent of either internal variability or changes to external forcing' [87]) has to be removed. Control simulations with fixed preindustrial greenhouse gas concentrations (piControl [88–102]) are used to estimate model drift, starting from the point at which the historical simulation departs from the piControl simulation and extending 250 years thereafter. From these control runs, the long-term trend over the historical and future time periods is calculated, and then removed from the simulations.

The SSP scenarios correspond to different climate forcing levels by 2100 [103]. Three scenarios are considered: SP1-2.6, SSP2-4.5 and SSP5-8.5 corresponding to climate forcing levels of 2.6, 4.5 and 8.5 W m^{-2}. Comparisons of the historical simulations are made against future projections for 2080–2099. To determine statistical significance in these differences, a Kolmogorov-Smirnov test was used at the 5% significance level.

3.2.1. Mean dynamic sea-level

In projections of the mean dynamic sea-level change under the SSP5-8.5 scenario, the global outlook shows an increase in most of the Northern Hemisphere, strongest over the North Atlantic, which is balanced by a decrease in the Southern Ocean (figure S4 [104],). The MMM changes in dynamic sea-level are significant at 5% under all SSP scenarios and for all UK boxes (figures 4(a) and (b)). Under SSP5-8.5, the MMM dynamic sea-level increases by 17.9 cm, 21.5 cm, 16.0 cm, 21.4 cm and 15.6 cm for WCS,

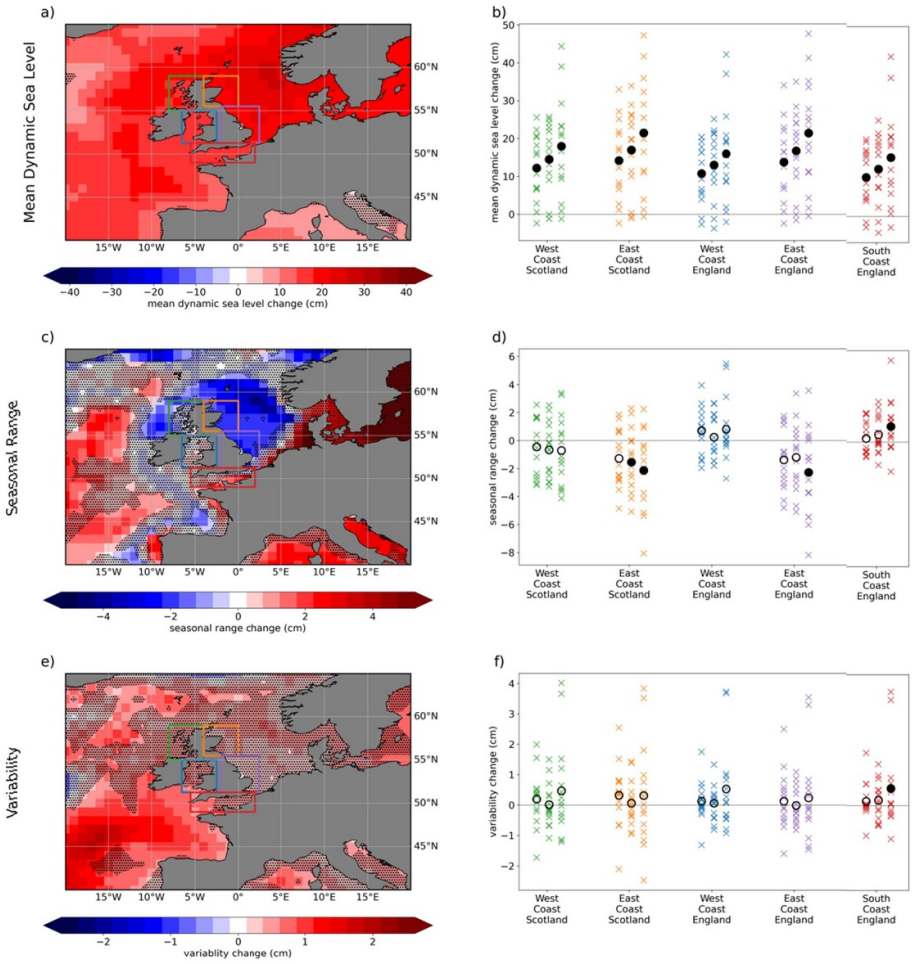

Figure 4. The CMIP6 MMM change in dynamic sea-level (a), seasonal range (c) and interannual variability (e) between the historical simulation (1993–2014) and SSP5-8.5 projection for 2080–2099, with UK boxes overlaid. Stippling shows areas where the correlations are insignificant at 5%. Changes under SSP1-2.6, SSP2-4.5 and SSP5-8.5 simulations in dynamic sea-level (b), seasonal range (d) and interannual variability (f) for each of the UK boxes. Each CMIP6 model is represented by a cross, with the MMM denoted by a black circle. Where the differences are significant, the black circle is solid.

ECS, WCE, ECE and SCE respectively. The majority of the models used in this study predict a future rise in dynamic sea-level, whilst a few show a small decrease.

3.2.2. Seasonal cycle

The seasonal range in dynamic sea-level projected for the SSP5-8.5 scenario decreases in the North Sea by over 2 cm (locally by 4 cm), whilst increasing non-significantly along the northern European coastline and in the English Channel (figure 4(c)). Within the UK boxes, the decrease in seasonal range is significant only for ECS and ECE with a 2.1 cm and 2.3 cm decrease respectively (figure 4(d)). In SCE, an increase of 1.1 cm in the seasonal range is also significant. In the remaining boxes and under the less extreme scenarios the changes in seasonal range are not significant.

3.2.3. Interannual variability

The change in interannual dynamic sea-level variability is only found to be significant for SCE under the SSP8-5.8 scenario (figure 4(f)). Other regions globally do show significant changes in variability, including over the North Atlantic southwest of the UK. The significant change for SCE is caused by the north-eastern extent of this North Atlantic signal (figure 4(e)).

3.3. Factors related to future increases in dynamic sea-level

Where statistically significant differences were found in the projections of mean dynamic sea-level and seasonal range with respect to the reference period, we identify other variables that also change significantly on the same timescales. Cross-model correlations show that the most significant change in the models predicting large increases in mean dynamic sea-level was a weakening in the Atlantic Meridional Overturning Circulation (AMOC), where AMOC is computed as the maximum of the overturning stream function at 26 N (from meridional velocities). The same relationship was also found in [105] along the eastern North America and Arctic coastlines.

We investigate this relationship over the wider sub-polar gyre (80 W-0 E, 45–62 N) at the same latitude as the UK and including the western UK shelf seas. Using the CMIP6 models, the dynamic sea-level is divided into the barotropic and baroclinic components (figure S5), where the baroclinic component at any location is here defined as the change in the depth integrated specific volume anomaly relative to the global mean change, and the barotropic component is then obtained as the residual between the dynamic sea-level and the baroclinic component. Temperature and salinity contributions to the baroclinic component are calculated in a similar way to [105]. Excluding outliers, baroclinic effects dominate 2:1 (not shown). In models with a stronger AMOC reduction, the sub-polar gyre is relatively cool and fresh, with the density reduction by freshening outcompeting the density increase associated with cooling. This is consistent with the mechanism proposed by [106] whereby the sea-level increase is due to a combination of changing surface fluxes of heat (reduced heat loss) and freshwater (increasing precipitation, reduced evaporation), coupled with a reduced oceanic supply of heat and salt to the sub-polar gyre caused by a weaker AMOC. Cross-model variability in AMOC projections likely relate to the model-specific details of wind, air-sea temperature and humidity differences over the sub-polar gyre [107]. Changes in wind stress curl and (turbulent) surface heat flux may be the reason for the coincident increase in barotropic sea-level.

Basin-wide dynamic sea-level signals in response to AMOC are consistent with those observed over the UK shelf-seas but deep-water signals are not readily translated to the shelf-seas due to the slope current along the western and northern boundaries of the British Isles [107]. As demonstrated by [106] the response of the shallow shelf regions to sea level changes over the deep ocean is dominated by mass fluxes between the deeper water and shelf seas. The mechanism by which this signal is communicated is not fully understood but is likely to be a combination of inshore wind-driven waters, breaks in the slope current due to deeper topography and circulation of water onto the shelf-sea to the north where the slope current is weaker [108].

Cross-model comparisons were also made of dynamic sea-level response to atmospheric JL between the historical and future simulations (figure S6). Although both the observations and models show a strong inter-annual correlation over the North Sea between SLA and JL, the cross-model comparisons do not indicate a significant correlation between SLA and JL between the reference and future simulation periods. This may indicate that the models respond differently to mean state changes in the JL than to interannual variability, or that the signal in response to the JL is masked by the larger signal from AMOC.

4. Storylines for future dynamic sea-level rise and storm surge risk in the UK

4.1. Dynamic storylines

We can combine our understanding of past, present and future changes in dynamic sea-level from the satellite observations and CMIP6 models to determine storylines for plausible future sea-level scenarios around the UK. The JL index (section 2) was found to be a good proxy for the interannual variability in the SLA caused by changes in wind stress. The further north that the jet moves, the higher the SLA anomaly over the North Sea adjacent to the ECE and ECS boxes. The rationale for selecting this variable as one of the building blocks for storylines is the robust poleward jet shift projected in future (although the magnitude of this is uncertain [24]).

Our second variable as determined from the CMIP6 projections is AMOC as most models showed a strong negative correlation between AMOC strength and dynamic sea-level. We would not expect to be able to see the same relationship in the observations due to the relatively long timescale of the AMOC compared to the length of the satellite data record.

Our storylines focus on the possible future changes in autumn SLA. This is when sea-level is at a maximum around the UK and where additional rises could have the greatest impact on the magnitude of storm surges and flooding events. We define two scenarios for the projected northward movement in the JL in autumn (SON) between the reference and future periods. This is evaluated using 13 of the 15 CMIP6 models where appropriate data are available. The mean northward movement is 1.82 degrees with a standard deviation of 1.26 degrees. We select 0.56 degrees as the minimum shift (using the MMM minus one standard deviation) and 3.08 degrees as the maximum shift (using the MMM plus one standard deviation). The difference in SLA resulting from a northward shift of the jet is calculated using the local regression coefficient for the observed detrended and deseasonalised SLA against the JL index in October.

To define a lower and upper bound for the change in AMOC, we first select the five models with the smallest change and the five models with the greatest change, and then take the MMM of these two sets of five models. This gives a minimum reduction in AMOC of −3.6 Sv and a maximum reduction of −10.7 Sv. We verify that these values represent approximately plus/minus one standard deviation from the mean for consistency with the JL index shift (−3.4 Sv and −10.1 Sv respectively) but use the MMMs of the two sets of five models in order to obtain the local changes in SLA. The changes in SLA for the five UK boxes are calculated as the MMM SLA from the two sets of five models.

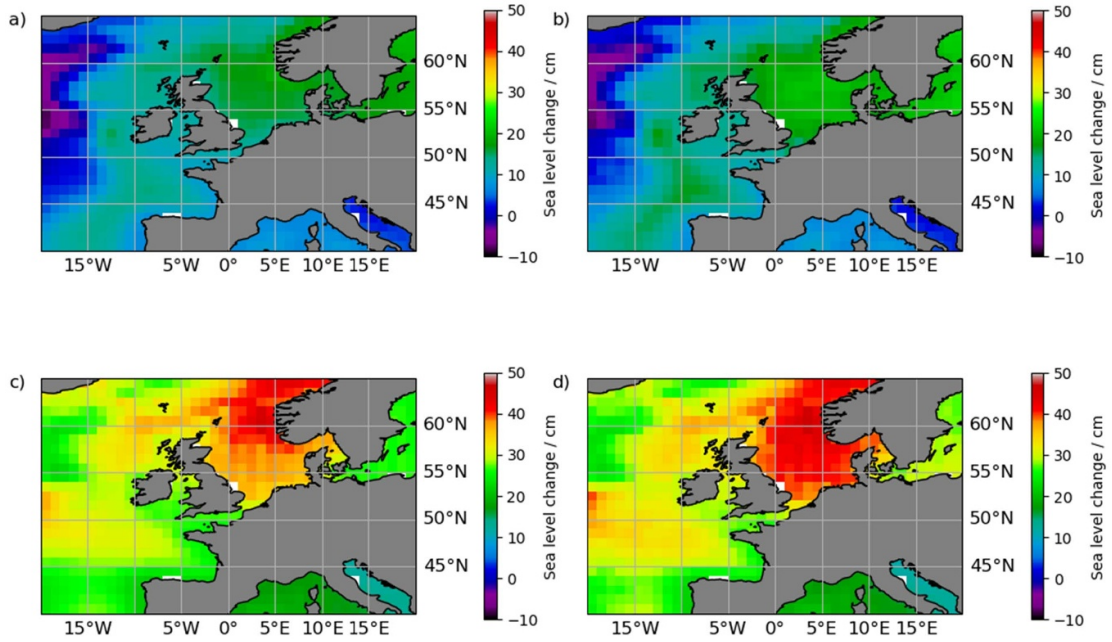

Figure 5. Storyline projections for future dynamic sea-level rise between 2080–2099. (a) Storyline 1: minimum shift in JL index and minimum reduction in AMOC. (b) Storyline 2: maximum shift in JL index and minimum reduction in AMOC. (c) Storyline 3: minimum shift in JL index and maximum reduction in AMOC. (d) Storyline 4: maximum shift in JL index and maximum reduction in AMOC. White squares on the map indicate boxes where either the SLA observations or future AMOC projections were unavailable.

Table 2. Projected dynamic sea-level rises for the five boxes around the UK coast under the 4 different storylines. All values are rounded to one decimal place (or one significant figure as appropriate) so there may be a small discrepancy between the totals and the sum of the components.

	Storyline 1 sea-level change (cm)			Storyline 2 sea-level change (cm)			Storyline 3 sea-level change (cm)			Storyline 4 sea-level change (cm)		
	AMOC	JL	Total	AMOC	JL	Total	AMOC	JL	Total	AMOC	JL	Total
WCS	12.3	0.4	12.7	12.3	2.0	14.3	30.0	0.4	30.4	30.0	2.0	32.0
ECS	14.2	0.5	14.7	14.2	2.9	17.1	34.9	0.5	35.4	34.9	2.9	37.8
WCE	11.0	0.4	11.4	11.0	2.1	13.1	28.0	0.4	28.4	28.0	2.1	30.1
ECE	14.3	0.7	15.0	14.3	4.0	18.3	35.0	0.7	35.7	35.0	4.0	39.0
SCE	10.2	0.3	10.5	10.2	1.7	11.8	26.4	0.3	26.7	26.4	1.7	28.1

We combine these four values to generate four storylines:

- Storyline 1: minimum shift in JL index and minimum reduction in AMOC (0.56 degrees north and −3.6 Sv respectively).
- Storyline 2: maximum shift in JL index and minimum reduction in AMOC (3.08 degrees north and −3.6 Sv respectively).
- Storyline 3: minimum shift in JL index and maximum reduction in AMOC (0.56 degrees north and −10.7 Sv respectively).
- Storyline 4: maximum shift in JL index and maximum reduction in AMOC (3.08 degrees north and −10.7 Sv respectively).

The projected changes in dynamic sea-level under these four storylines are shown in both figure 5 and table 2. To make the comparison, the SLA observations are re-gridded at one-degree resolution, consistent with the model output. To compare regional values, we use all one-degree grid-box centres that fall within the bounds of the UK boxes (table 1). Considering first the total change in dynamic sea-level, the largest increases occur over the North Sea and under storyline 4, with a maximum rise of 39.0 cm in ECE and 37.8 cm in ECS by 2080–2099. The smallest increases in dynamic sea-level are seen under storyline 1 in SCE and WCE, with increases of 10.5 and 11.4 cm respectively. The spatial distribution of the dynamic sea-level rise is dominated largely by the AMOC signal and in SCE, WCE and WCS the contribution from the northward movement of the jet stream is typically ∼0.5 cm. On the east coast of the UK the JL index is a more important indicator of changes in dynamic sea-level (although the response is smaller than that related to changes in AMOC). Under the upper bound conditions imposed

Table 3. Maximum dynamic sea-level elevation above the mean sea-level for the reference (historical) and future time periods caused by local seasonal and interannual variability. Dynamic sea-level rise is calculated using the MMM of the five models showing the maximum (max) and minimum (min) dynamic sea-level rise for each of the components in equations (2) and (3): seasonal range, interannual variability and the MMM difference between the historical and future simulations.

		West Coast England (WCE)	South Coast England (SCE)	East Coast England (ECE)	West Coast Scotland (WCS)	East Coast Scotland (ECS)
Reference worst case (cm)	Max E_h	13.8	13.1	20.3	17.1	20.0
	Min E_h	8.3	8.1	12.5	9.5	10.3
SSP5-8.5 worst case (cm)	Max E_f	47.4	46.7	57.6	51.5	57.6
	Min E_f	12.0	11.2	17.5	13.9	15.2

in storylines 2 and 4, this component accounts for a 4.0 and 2.9 cm rise in dynamic sea-level for ECE and ECS respectively (table 2).

In addition to the storylines defined above, it is also possible to use the CMIP6 models to determine an extreme dynamic sea-level response (or worst-case scenario) given the projected changes to the mean, seasonal range and interannual variability in dynamic sea-level, which can be compared with the worst-case scenario calculated for the reference period (from the historical CMIP6 simulations). We define extreme cases using the following equations:

$$E_h = \frac{\max(SR_h)}{2} + 3(\max(\sigma_h)) \quad (3)$$

$$E_f = \max(MMM_f - MMM_h) + \frac{\max(SR_f)}{2} + 3(\max(\sigma_f)). \quad (4)$$

MMM is the multi-model-mean dynamic sea-level, *SR* the seasonal range and σ the dynamic sea-level variability. The subscripts 'h' and 'f' denote 'historical' and 'future' respectively. The maximum is defined as the mean of the five models with the most extreme change for each metric separately (mean change, seasonal range and variability). This is a pragmatic choice as the most extreme model predictions would be less likely to occur. The equivalent can also be calculated for the minimum using the five models with the smallest changes in each metric. This approach provides a 'worse case' scenario for dynamic sea-level rise that would occur in addition to current mean sea-level projections (as these do not include seasonal and interannual variability).

This approach differs from the storylines shown in figure 5 and table 2. The storylines are linked directly to two different physical climate responses (changes to JL and changes in AMOC), whereas this approach summarises the maximum modelled changes to dynamic sea-level which may result from different combinations of physical processes. Table 3 shows E_h and E_f for each of the UK boxes. Consistent with the results of the storylines, the greatest dynamic sea-level rise occurs along the east coast of the UK. For the historical case, the maximum dynamic sea-level increase above the mean sea-level is 20.3 cm for ECE and 20.0 cm for ECS. For the future time period, this increases significantly to 57.6 cm for ECE and ECS, which is 20 cm greater than the maximum dynamic sea-level rise calculated using the storylines.

In all the UK boxes, the 'worst-case' dynamic sea-level increase above the mean more than doubles between the reference and future periods when considering the maximum. Considering the models with the minimum seasonal range and interannual variability, the 'worst-case' scenarios are still largest along the east coast, but more modest in size: 12.5 cm and 10.3 cm respectively for ECE and ECS for the reference time period. The relative change between the reference and future periods is also smaller with a ~5 cm change in each location, giving a total of 17.5 and 15.2 cm in ECE and ECS respectively.

4.2. Event storyline

We illustrate the potential impact and importance of local dynamic sea-level rise to coastal flooding using an idealised example based on the storm that occurred on 5 December 2013. We focus on ECE where the projected increase in dynamic sea-level by 2080–2099 is largest and there are extensive areas of low-lying ground close to the coast. The idealised example considers what the relative differences would be to coastal flood risk if the storm surge of 2013 were to occur in 2100. To make this comparison we use a high-resolution LiDAR survey of England [109] (re-gridded from 10 m to 100 m spatial resolution using the minimum altitude) to define the current elevation of ECE and neighbouring inland areas relative to the MSL.

Our basis for defining the 'current day' flood risk under storm surge conditions of 2013 is to use a maximum elevation of water above MSL defined as half the maximum tidal range on the east coast (2 m [110]) plus the skew-surge height measured at Lowestoft in the 2013 storm (2.06 m [111]). In this simplistic model, the assumption is that all ground below 4.06 m along the ECE coastline would be at risk of flooding. The area potentially affected under this scenario is shown in figure 6 (beige) and encompasses in-land regions around the Wash, Humber Estuary and Thames Estuary as well as the coastline of Essex, Suffolk, Norfolk, Lincolnshire and Yorkshire.

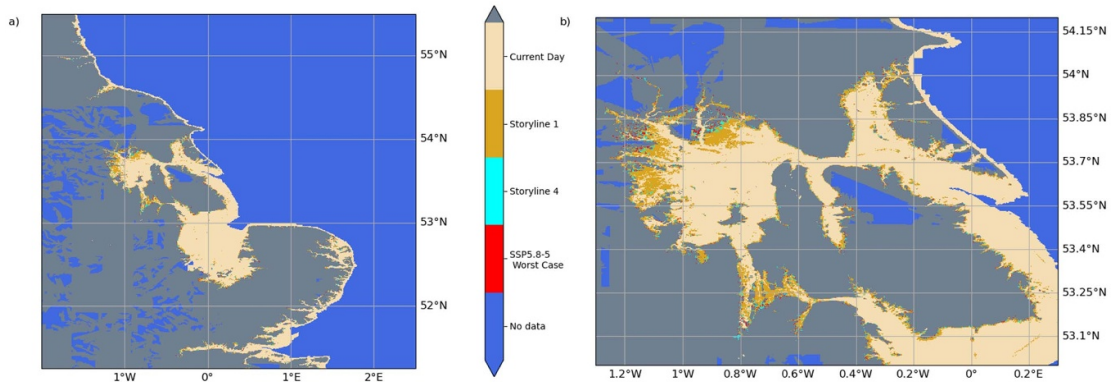

Figure 6. Idealised flood-risk example based on the storm surge of the 5 December 2013. Figures show land below the maximum surge height for (a) ECE and (b) Humber Estuary under current day conditions compared with storyline 1, storyline 4 and SSP5-8.5 worst case scenarios. Ocean and areas with no LiDAR survey data available are shown in blue. Note that this figure is not generated using an inundation model and should only be interpreted as indicative of relative risk.

Considering future scenarios, a further 1.82 m is added to the MSL as a result of sea-level rise (which includes ice mass change, thermosteric and dynamic sea-level and isostatic rebound as modelled by CMIP5 [112]). This estimate also closely matches the IPCC projection under the SSP5-8.5 low-likelihood, high-impact storyline [113]. The authors note that this IPCC projection is a low-confidence scenario, but feel it is appropriate to use in the context of constructing storylines. The 83rd percentile is a 1.6 m sea-level rise and the 95th percentile approaches a 2.5 m sea-level rise by 2100. For comparison, the medium confidence SSP5-8.5 scenario has a median value of 0.77 m and likely range of 0.63–1.01 m [2]. Dynamic sea-level rise is added for storyline 1 (15.0 cm), storyline 4 (39.0 cm) and the SSP5-8.5 worst case scenario (57.6 cm). The further 'at risk' areas as defined by this experiment are shown as gold (storyline 1), cyan (storyline 4) and red (SSP5-8.5 worst case) in figure 6. The worst-case scenario represents a 2% increase in total flooded area over the current day representation. The biggest changes are seen between the current day and storyline 1 (81.9% of the total), particularly around the Humber Estuary (figure 6(b)). Of this, 94.8% of the increase results from the non-dynamic component, and 5.2% from dynamic sea-level rise. A further 10.8% of the increase of 'at risk' land is accounted for by the transition from Storyline 1 to Storyline 4 with the remaining 7.3% occurring between Storyline 4 and the worst-case scenario. Under the worst-case scenario, the spatial extent of land considered 'at risk' increases by 1414 km^2 over the current day, using this simplistic model. 22.4% of the additional land 'at risk' under the worst-case scenario can be attributed to changes in dynamic sea level.

5. Discussion and conclusions

This paper draws together both satellite altimetry and CMIP6 model projections to better understand future dynamic sea-level rise in the UK shelf-seas. Recent observations are analysed to characterise seasonal and interannual variability in SLA (section 2). This approach focuses on a local shallow water region (rather than a large ocean basin) and aims to characterise short-term variability often neglected in sea-level projections. CMIP6 model skill is assessed with reference to the satellite altimetry and found to be sufficient to indicate the possible range in regional variability in dynamic sea-level (section 3). Interannual variability in the satellite altimetry is driven by the atmospheric JL and future changes in dynamic sea-level within the model are most closely correlated with a weakening AMOC. We construct storylines based on these two drivers of variability (section 4) to better understand the local variations in dynamic sea-level rise around the UK coast by 2080–2099. This approach is novel as it combines both greenhouse gas projections in the CMIP6 models and climate response.

Of the two drivers used to construct the storylines, AMOC has the greater effect on dynamic sea-level projections, with the largest dynamic sea-level rise observed over the north eastern North Sea. Northward movement of the jet stream raises the dynamic sea-level closer to the eastern coast of the UK where the lowest-lying land is found. JL varies more rapidly than AMOC, with a range of $\sim \pm 8°$ over the reference period. As a consequence, interannual variability in the JL in addition to a mean northward shift (as explored in the storylines) could give a greater rise in dynamic sea-level locally than shown in figure 5, which may be important in the event of a storm surge, particularly if coupled also with high tide. Any change to the future variability of the jet stream latitude would also affect local dynamic sea-level.

The worst case scenarios and idealised example are included to demonstrate the impact of rising sea-level on the possible scale of flooding events and importance of local variability in dynamic sea-level in

determining impacts such as the breaching of coastal defences. The idealised example focuses on the spatial extent of land that might be considered 'at risk' but the other important factor is the return time of flooding events. Higher sea-levels increase the probability of flooding events occurring, reducing the return times of more serious inundations [114, 115]. It may also be further compounded by changes in storm frequency, intensity or track although there is considerable uncertainty in the projected changes to storms over the next 80 years [116].

Although illustrative, this idealised example is not predictive of potentially flooded land by 2100. To fully understand the spatial extent of at-risk lands would require the use of an innundation model that factors in the local topography, coastal defences and reduction of wave height as flood water moves inland [111, 117], meaning that figure 6 is a likely overestimate of the spatial extent but more indicative of the relative risk. The severity of storm surge events are also dependent on the tide level and wind direction as well as local geology and susceptibility to coastal erosion [111].

Analysis of observations and CMIP6 model projections in this paper shows the importance of quantifying local, dynamic variability in sea-level in addition to mean sea-level change from thermosteric and ice mass contributions. Future sea-level rise is dependent not only on the emission scenario and extent of atmospheric warming, but also on the response of the climate system to these changes. The projected northward migration of the jet stream and reduction in AMOC both have the potential to increase dynamic sea-level. Further studies linking climate response to future warming scenarios, for which the storyline framework can be used, are required to fully understand the impact of sea-level rise on coastal populations and infrastructure.

Data availability statement

The data that support the findings of this study are available upon reasonable request from the authors.

Acknowledgments

The authors received funding for this paper from the Natural Environment Research Council (NERC) as part of the North Atlantic Climate System Integrated Study (ACSIS) under Grant Nos. NE/N018052/1, NE/N018001/1 and NE/N018044/1.

This work has received funding from the European Union's Horizon 2020 research and innovation programme under Grant Agreement No. 820989 (project COMFORT, Our common future ocean in the Earth system—quantifying coupled cycles of carbon, oxygen and nutrients for determining and achieving safe operation spaces with respect to tipping points). The work reflects only the authors' view; the European Commission and their executive agency are not responsible for any use that may be made of the information the work contains.

This work used JASMIN, the UK's collaborative data analysis environment (https://jasmin.ac.uk).

ORCID iDs

Claire E Bulgin https://orcid.org/0000-0003-4368-7386
Jennifer V Mecking https://orcid.org/0000-0002-1834-1845
Ben J Harvey https://orcid.org/0000-0002-6510-8181
Svetlana Jevrejeva https://orcid.org/0000-0001-9490-4665
Christopher J Merchant https://orcid.org/0000-0003-4687-9850
Bablu Sinha https://orcid.org/0000-0002-7303-3175

References

[1] Fox-Kemper B *et al* 2021 Ocean, cryosphere and sea level change. Chapter in: climate change 2021: the physical science basis. Contribution of working group 1 to the sixth assessment report of the intergovermental panel on climate change (Cambridge University Press)
[2] Masson-Dellmotte V *et al* 2021 IPCC 2021: summary for policy makers. In: climate change 2021: the physical science basis. Contribution of working group 1 to the sixth assessment report of the intergovermental panel on climate change (Cambridge University Press)
[3] Jevrejeva S, Palanisamy H and Jackson L P 2021 Global mean thermosteric sea level projections by 2100 in CMIP6 models *Environ. Res. Lett.* **16** 014028
[4] Vousdoukas M I, Mentaschi L, Voukouvalas E, Verlaan M, Jevrejeva S, Jackson L P and Feyen L 2018 Global probabilistic projections of extreme sea levels show intensification of coastal flood hazard *Nat. Commun.* **9** 2360
[5] Tebaldi C, Ranasinghe R, Vousdoukas M, Rasmussen D J, Vega-Westhoff B, Kirezci E, Kopp R E, Sriver R and Mentaschi L 2021 Extreme sea levels at different global warming levels *Nat. Clim. Change* **11** 746–51
[6] Eyring V, Bony S, Meehl G A, Senior C A, Stevens B, Stouffer R J and Taylor K E 2016 Overview of the coupled model intercomparison project phase 6 (CMIP6) experimental design and organization *Geosci. Model Dev.* **9** 1937–58
[7] Carson M, Köhl A, Stammer D, Slangen A B A, Katsman C A, van de Wal R S W, Church J and White N 2016 Coastal sea level changes, observed and projected during the 20th and 21st century *Clim. Change* **134** 269–81
[8] Qu Y, Liu Y, Jevrejeva S and Jackson L P 2020 Future sea level rise along the coast of China and adjacent region under 1.5 °C and 2 °C global warming *Adv. Clim. Change Res.* **11** 227–38
[9] Shepherd T *et al* 2018 Storylines: an alternative approach to representing uncertainty in physical aspects of climate change *Clim. Change* **151** 555–71
[10] Jevrejeva S, Jackson L P, Grinsted A, Lincke D and Marzeion B 2018 Flood damage costs under the sea level rise with warming of 1.5 °C and 2 °C *Environ. Res. Lett.* **13** 074014
[11] Pörtner H-O *et al* (ed) 2022 IPCC summary for policymakers in climate change 2022: impacts, adaptation, and vulnerability. Contribution of working group II to the

sixth assessment report of the Intergovernmental Panel on Climate Change (Cambridge University Press)
[12] Brown S et al 2021 Global costs of protecting against sea-level rise at 1.5–4.0 °C Clim. Change 167 4
[13] Sigmond M, Fyfe J C, Saenko O A and Swart N C 2020 Ongoing AMOC and related sea-level and temperature changes after achieving the Paris targets Nat. Clim. Change 10 672
[14] Robson J et al 2018 Recent multivariate changes in the North Atlantic climate system, with a focus on 2005–2016 Int. J. Climatol. 38 5050–76
[15] Williams J, Horsburgh K J, Williams J A and Proctor R N F 2014 Tide and skew surge independence: new insights for flood risk Geophys. Res. Lett. 43 6410–7
[16] ESA Sea Level CCI project team 2017 ESA sea level climate change initiative (Sea_Level_cci): fundamental climate data records of sea level anomalies and altimeter standards Version 2.0. Centre of Environmental Data Analysis (available at: https://catalogue.ceda.ac.uk/uuid/2785ee1ec6274be39d11e7e7ce51b381)
[17] Quartly G D et al 2017 A new phase in the production of quality-controlled sea level data Earth Syst. Sci. Data 9 557–72
[18] Ponte R M 2006 Low-frequency sea level variability and the inverted barometer effect J. Atmos. Ocean Technol. 23 619–29
[19] Thomson R E and Fine I V 2021 Revisiting the ocean's nonisostatic response to 5-day atmospheric loading: new results based on global bottom pressure records and numerical modeling J. Phys. Oceanogr. 51 2845–59
[20] Hersbach H et al 2020 The ERA5 global reanalysis Q. J. R. Meteorol. Soc. 146 1999–2049
[21] O'Connor W P, Chao B F, Zheng D and Au A Y 2000 Wind stress forcing of the North Sea 'pole tide' Geophys. J. Int. 142 620–30
[22] Winther N G and Johannessen J A 2006 North Sea circulation: Atlantic inflow and its destination J. Geophys. Res. 111 C12018
[23] Woolings T, Hannachi A and Hoskins B 2010 Variability of the North Atlantic eddy-driven jet stream Q. J. R. Meteorol. Soc. 136 856–68
[24] Harvey B, Hawkins E and Sutton R 2023 Storylines for future changes of the North Atlantic jet and associated impacts on the UK (in preparation)
[25] Ceppi P, Selinka M D and Hartmann D L 2014 The response of the Southern Hemispheric eddy-driven jet to future changes in shortwave radiation in CMIP5 Geophys. Res. Lett. 41 3244–50
[26] Kendon M, McCarthy M, Jevrejeva S, Matthews A, Sparks T and Garforth J 2021 State of the UK Climate 2020 Int. J. Climatol. 41 S2
[27] Ablain M, Meyssignac B, Zawadzki L, Jugier R, Ribes A, Spada G, Benveniste J, Cazanave A and Picot N 2019 Uncertainty in satellite estimates of global mean sea-level changes, trend and acceleration Earth Syst. Sci. Data 11 1189–202
[28] Lawrence B N, Bennett V L, Churchill J, Juckes M, Kershaw P, Pascoe S, Pepler S, Pritchard M and Stephens A 2013 Storing and manipulating environmental big data with JASMIN IEEE Int. Conf. on Big Data (Silicon Valley, CA, 6–9 October 2023) pp 68–75
[29] Rong X 2019a CAMS CAMS_CSM1.0 model output prepared for CMIP6 CMIP historical Version 20190708 Earth System Grid Federation (https://doi.org/10.22033/ESGF/CMIP6.9754)
[30] Rong X 2019b CAMS CAMS_CSM1.0 model output prepared for CMIP6 ScenarioMIP ssp126x Version 20190708 Earth System Grid Federation (https://doi.org/10.22033/ESGF/CMIP6.11046)
[31] Rong X 2019c CAMS CAMS_CSM1.0 model output prepared for CMIP6 ScenarioMIP ssp245 Version 20190807 Earth System Grid Federation (https://doi.org/10.22033/ESGF/CMIP6.11047)
[32] Rong X 2019d CAMS CAMS_CSM1.0 model output prepared for CMIP6 ScenarioMIP ssp585 Version 20190807 Earth System Grid Federation (https://doi.org/10.22033/ESGF/CMIP6.11052)
[33] Chai Z 2020a CAS CAS-ESM1.0 model output prepared for CMIP6 CMIP historical Version 20201228 Earth System Grid Federation (https://doi.org/10.22033/ESGF/CMIP6.3353)
[34] Danabasoglu G 2019a NCAR CESM2-WACCM-FV2 model output prepared for CMIP6 CMIP historical Version 20190808 Earth System Grid Federation (https://doi.org/10.22033/ESGF/CMIP6.11298)
[35] Danabasoglu G 2019b NCAR CESM2-WACCM-FV2 model output prepared for CMIP6 ScenarioMIP ssp126 Version 20210211 Earth System Grid Federation (https://doi.org/10.22033/ESGF/CMIP6.10100)
[36] Danabasoglu G 2019c NCAR CESM2-WACCM-FV2 model output prepared for CMIP6 ScenarioMIP ssp245 Version 20190815 Earth System Grid Federation (https://doi.org/10.22033/ESGF/CMIP6.10101)
[37] Danabasoglu G 2019d NCAR CESM2-WACCM-FV2 model output prepared for CMIP6 ScenarioMIP ssp585 Version 20200702 Earth System Grid Federation (https://doi.org/10.22033/ESGF/CMIP6.10115)
[38] Huang W 2019a THU CIESM model output prepared for CMIP6 CMIP historical Version 20200220 Earth System Grid Federation (https://doi.org/10.22033/ESGF/CMIP6.8843)
[39] Huang W 2019b THU CIESM model output prepared for CMIP6 ScenarioMIP ssp126 Version 20200220 Earth System Grid Federation (https://doi.org/10.22033/ESGF/CMIP6.8857)
[40] Huang W 2019c THU CIESM model output prepared for CMIP6 ScenarioMIP ssp245 Version 20200220 Earth System Grid Federation (https://doi.org/10.22033/ESGF/CMIP6.8858)
[41] Huang W 2019d THU CIESM model output prepared for CMIP6 ScenarioMIP ssp585 Version 20200220 Earth System Grid Federation (https://doi.org/10.22033/ESGF/CMIP6.8863)
[42] Lovato T, Peano D and Butenschoen M 2021a CMCC CMCC-ESM2 model output prepared for CMIP6 CMIP historical Version 20210114 Earth System Grid Federation (https://doi.org/10.22033/ESGF/CMIP6.13195)
[43] Lovato T, Peano D and Butenschoen M 2021b CMCC CMCC-ESM2 model output prepared for CMIP6 ScenarioMIP ssp126 Version 20210126 Earth System Grid Federation (https://doi.org/10.22033/ESGF/CMIP6.13250)
[44] Lovato T, Peano D and Butenschoen M 2021c CMCC CMCC-ESM2 model output prepared for CMIP6 ScenarioMIP ssp245 Version 20210129 Earth System Grid Federation (https://doi.org/10.22033/ESGF/CMIP6.13252)
[45] Lovato T, Peano D and Butenschoen M 2021d CMCC CMCC-ESM2 model output prepared for CMIP6 ScenarioMIP ssp585 Version 20210126 Earth System Grid Federation (https://doi.org/10.22033/ESGF/CMIP6.13259)
[46] EC-Earth Consortium 2019a EC-earth-consortium EC-Earth3 model output prepared for CMIP6 CMIP historical Version 20200918 Earth System Grid Federation (https://doi.org/10.22033/ESGF/CMIP6.4700)
[47] EC-Earth Consortium 2019b EC-earth-consortium EC-Earth3 model output prepared for CMIP6 ScenarioMIP ssp126 Version 20200918 Earth System Grid Federation (https://doi.org/10.22033/ESGF/CMIP6.4874)
[48] EC-Earth Consortium 2019c EC-earth-consortium EC-Earth3 model output prepared for CMIP6 ScenarioMIP ssp245 Version 20200918 Earth System Grid Federation (https://doi.org/10.22033/ESGF/CMIP6.4880)
[49] EC-Earth Consortium 2019d EC-earth-consortium EC-Earth3 model output prepared for CMIP6

ScenarioMIP ssp585 Version 20200918 *Earth System Grid Federation* (https://doi.org/10.22033/ESGF/CMIP6.4912)
[50] Song Z, Qiao F, Bao Y, Shu Q, Song Y and Yang X 2019a FIO-QLNM FIO-ESM2.0 model output prepared for CMIP6 CMIP historical Version 20191122 *Earth System Grid Federation* (https://doi.org/10.22033/ESGF/CMIP6.9199)
[51] Song Z, Qiao F, Bao Y, Shu Q, Song Y and Yang X 2019b FIO-QLNM FIO-ESM2.0 model output prepared for CMIP6 ScenarioMIP ssp126 Version 20191227 *Earth System Grid Federation* (https://doi.org/10.22033/ESGF/CMIP6.9208)
[52] Song Z, Qiao F, Bao Y, Shu Q, Song Y and Yang X 2019c FIO-QLNM FIO-ESM2.0 model output prepared for CMIP6 ScenarioMIP ssp245 Version 20191227 *Earth System Grid Federation* (https://doi.org/10.22033/ESGF/CMIP6.9209)
[53] Song Z, Qiao F, Bao Y, Shu Q, Song Y and Yang X 2019d FIO-QLNM FIO-ESM2.0 model output prepared for CMIP6 ScenarioMIP ssp585 Version 20191227 *Earth System Grid Federation* (https://doi.org/10.22033/ESGF/CMIP6.9214)
[54] Ridley J, Menary M, Kuhlbrodt T, Andrews M and Andrews T 2019a MOHC HadGEM3-GC31-LL model output prepared for CMIP6 CMIP historical Version 20190624 *Earth System Grid Federation* (https://doi.org/10.22033/ESGF/CMIP6.6109)
[55] Good P 2020a MOHC HadGEM3-GC31-LL model output prepared for CMIP6 ScenarioMIP ssp126 Version 20200114 *Earth System Grid Federation* (https://doi.org/10.22033/ESGF/CMIP6.10849)
[56] Good P 2019 MOHC HadGEM3-GC31-LL model output prepared for CMIP6 ScenarioMIP ssp245 Version 20190908 *Earth System Grid Federation* (https://doi.org/10.22033/ESGF/CMIP6.10851)
[57] Good P 2020b MOHC HadGEM3-GC31-LL model output prepared for CMIP6 ScenarioMIP ssp585 Version 20200114 *Earth System Grid Federation* (https://doi.org/10.22033/ESGF/CMIP6.10901)
[58] Boucher O *et al* 2018a IPSL IPSL-CM6A-LR model output prepared for CMIP6 CMIP historical Version 20180803 *Earth System Grid Federation* (https://doi.org/10.22033/ESGF/CMIP6.5195)
[59] Boucher O *et al* 2019a IPSL IPSL-CM6A-LR model output prepared for CMIP6 ScenarioMIP ssp126 Version 20190903 *Earth System Grid Federation* (https://doi.org/10.22033/ESGF/CMIP6.5262)
[60] Boucher O *et al* 2019b IPSL IPSL-CM6A-LR model output prepared for CMIP6 ScenarioMIP ssp245 Version 20190119 *Earth System Grid Federation* (https://doi.org/10.22033/ESGF/CMIP6.5264)
[61] Boucher O *et al* 2019c IPSL IPSL-CM6A-LR model output prepared for CMIP6 ScenarioMIP ssp585 Version 20190903 *Earth System Grid Federation* (https://doi.org/10.22033/ESGF/CMIP6.5271)
[62] Jungclaus J *et al* 2019a MPI-M MPI-ESM1.2-HR model output prepared for CMIP6 CMIP historical Version 20190710 *Earth System Grid Federation* (https://doi.org/10.22033/ESGF/CMIP6.6594)
[63] Schupfner M *et al* 2019a DKRZ MPI-ESM1.2-HR model output prepared for CMIP6 ScenarioMIP ssp126 Version 20190710 *Earth System Grid Federation* (https://doi.org/10.22033/ESGF/CMIP6.4397)
[64] Schupfner M *et al* 2019b DKRZ MPI-ESM1.2-HR model output prepared for CMIP6 ScenarioMIP ssp245 Version 20190710 *Earth System Grid Federation* (https://doi.org/10.22033/ESGF/CMIP6.4398)
[65] Schupfner M *et al* 2019c DKRZ MPI-ESM1.2-HR model output prepared for CMIP6 ScenarioMIP ssp585 Version 20190710 *Earth System Grid Federation* (https://doi.org/10.22033/ESGF/CMIP6.4403)
[66] Weiners K-H *et al* 2019a MPI-M MPI-ESM1.2-LR model output prepared for CMIP6 CMIP historical Version 20190710 *Earth System Grid Federation* (https://doi.org/10.22033/ESGF/CMIP6.6595)
[67] Weiners K-H *et al* 2019b MPI-M MPI-ESM1.2-LR model output prepared for CMIP6 ScenarioMIP ssp126 Version 20190710 *Earth System Grid Federation* (https://doi.org/10.22033/ESGF/CMIP6.6690)
[68] Weiners K-H *et al* 2019c MPI-M MPI-ESM1.2-LR model output prepared for CMIP6 ScenarioMIP ssp245 Version 20190710 *Earth System Grid Federation* (https://doi.org/10.22033/ESGF/CMIP6.6693)
[69] Weiners K-H *et al* 2019d MPI-M MPI-ESM1.2-LR model output prepared for CMIP6 ScenarioMIP ssp585 Version 20190710 *Earth System Grid Federation* (https://doi.org/10.22033/ESGF/CMIP6.6705)
[70] Yukimoto S *et al* 2019a MRI MRI-ESM2.0 model output prepared for CMIP6 CMIP historical Version 20191205 *Earth System Grid Federation* (https://doi.org/10.22033/ESGF/CMIP6.6842)
[71] Yukimoto S *et al* 2019b MRI MRI-ESM2.0 model output prepared for CMIP6 ScenarioMIP ssp126 Version 20200222 *Earth System Grid Federation* (https://doi.org/10.22033/ESGF/CMIP6.6909)
[72] Yukimoto S *et al* 2019c MRI MRI-ESM2.0 model output prepared for CMIP6 ScenarioMIP ssp245 Version 20200222 *Earth System Grid Federation* (https://doi.org/10.22033/ESGF/CMIP6.6910)
[73] Yukimoto S *et al* 2019d MRI MRI-ESM2.0 model output prepared for CMIP6 ScenarioMIP ssp585 Version 20200120 *Earth System Grid Federation* (https://doi.org/10.22033/ESGF/CMIP6.6929)
[74] Seland O *et al* 2019a NCC NorESM2-LM model output prepared for CMIP6 CMIP historical Version 20190815 *Earth System Grid Federation* (https://doi.org/10.22033/ESGF/CMIP6.8036)
[75] Seland O *et al* 2019b NCC NorESM2-LM model output prepared for CMIP6 ScenarioMIP ssp126 Version 20191108 *Earth System Grid Federation* (https://doi.org/10.22033/ESGF/CMIP6.8248)
[76] Seland O *et al* 2019c NCC NorESM2-LM model output prepared for CMIP6 ScenarioMIP ssp245 Version 20191108 *Earth System Grid Federation* (https://doi.org/10.22033/ESGF/CMIP6.8253)
[77] Seland O *et al* 2019d NCC NorESM2-LM model output prepared for CMIP6 ScenarioMIP ssp585 Version 20191108 *Earth System Grid Federation* (https://doi.org/10.22033/ESGF/CMIP6.8319)
[78] Bentsen M *et al* 2019a NCC NorESM2-MM model prepared for CMIP6 CMIP historical Version 20191108 *Earth System Grid Federation* (https://doi.org/10.22033/ESGF/CMIP6.8040)
[79] Bentsen M *et al* 2019b NCC NorESM2-MM model prepared for CMIP6 ScenarioMIP sssp126 Version 20191108 *Earth System Grid Federation* (https://doi.org/10.22033/ESGF/CMIP6.8250)
[80] Bentsen M *et al* 2019c NCC NorESM2-MM model prepared for CMIP6 ScenarioMIP ssp245 Version 20191108 *Earth System Grid Federation* (https://doi.org/10.22033/ESGF/CMIP6.8255)
[81] Bentsen M *et al* 2019d NCC NorESM2-MM model prepared for CMIP6 ScenarioMIP ssp585 Version 20191108 *Earth System Grid Federation* (https://doi.org/10.22033/ESGF/CMIP6.8321)
[82] Tang Y, Rumbold S, Ellis R, Kelley D, Mulcahy J, Sellar A, Walton J and Jones C 2019b MOHC UKESM1.0-LL model output prepared for CMIP6 CMIP historical Version 20190627 *Earth System Grid Federation* (https://doi.org/10.22033/ESGF/CMIP6.6113)
[83] Good P, Sellar A, Tang Y, Rumbold S, Ellis R, Kelley D and Kuhlbrodt T 2019a MOHC UKESM1.0-LL model output prepared for CMIP6 ScenarioMIP ssp126 Version 20190708 *Earth System Grid Federation* (https://doi.org/10.22033/ESGF/CMIP6.6333)

[84] Good P, Sellar A, Tang Y, Rumbold S, Ellis R, Kelley D and Kuhlbrodt T 2019a MOHC UKESM1.0-LL model output prepared for CMIP6 ScenarioMIP ssp245 Version 20190507 *Earth System Grid Federation* (https://doi.org/10.22033/ESGF/CMIP6.6339)
[85] Good P, Sellar A, Tang Y, Rumbold S, Ellis R, Kelley D and Kuhlbrodt T 2019a MOHC UKESM1.0-LL model output prepared for CMIP6 ScenarioMIP ssp585 Version 20190726 *Earth System Grid Federation* (https://doi.org/10.22033/ESGF/CMIP6.6405)
[86] Griffies S M *et al* 2016 OMIP contribution to CMIP6: experimental and diagnostic protocol for the physical component of the ocean model intercomparison Project *Geosci. Model Dev.* **9** 3231–96
[87] Gupta A S, Jourdain N C, Brown J N and Monselesan D 2013 Climate drift in the CMIP5 Models *J. Clim.* **26** 8597–615
[88] Rong X 2019e CAMS CAMS_CSM1.0 model output prepared for CMIP6 CMIP piControl Version 20190729 *Earth System Grid Federation* (https://doi.org/10.22033/ESGF/CMIP6.9797)
[89] Chai Z 2020c CAS CAS-ESM1.0 model output prepared for CMIP6 CMIP piControl Version 20201227 *Earth System Grid Federation* (https://doi.org/10.22033/ESGF/CMIP6.3445)
[90] Danabasoglu G 2019e NCAR CESM2-WACCM-FV2 model output prepared for CMIP6 CMIP piControl Version 20190320 *Earth System Grid Federation* (https://doi.org/10.22033/ESGF/CMIP6.10094)
[91] Huang W 2019e THU CIESM model output prepared for CMIP6 CMIP piControl Version 20200220 *Earth System Grid Federation* (https://doi.org/10.22033/ESGF/CMIP6.8849)
[92] Lovato T, Peano D and Butenschoen M 2021e CMCC CMCC-ESM2 model output prepared for CMIP6 CMIP piControl Version 20210304 *Earth System Grid Federation* (https://doi.org/10.22033/ESGF/CMIP6.13241)
[93] EC-Earth Consortium 2019e EC-earth-consortium EC-Earth3 model output prepared for CMIP6 CMIP piControl Version 20200918 *Earth System Grid Federation* (https://doi.org/10.22033/ESGF/CMIP6.4842)
[94] Song Z, Qiao F, Bao Y, Shu Q, Song Y and Yang X 2019e FIO-QLNM FIO-ESM2.0 model output prepared for CMIP6 CMIP piControl Version 20200226 *Earth System Grid Federation* (https://doi.org/10.22033/ESGF/CMIP6.9205)
[95] Ridley J, Menary M, Kuhlbrodt T, Andrews M and Andrews T 2019b MOHC HadGEM3-GC31-LL model output prepared for CMIP6 CMIP piControl Version 20211103 *Earth System Grid Federation* (https://doi.org/10.22033/ESGF/CMIP6.6294)
[96] Boucher O *et al* 2018b IPSL IPSL-CM6A-LR model output prepared for CMIP6 CMIP piControlx Version 20211103 *Earth System Grid Federation* (https://doi.org/10.22033/ESGF/CMIP6.5251)
[97] Jungclaus J *et al* 2019b MPI-M MPI-ESM1.2-HR model output prepared for CMIP6 CMIP piControl Version 20190710 *Earth System Grid Federation* (https://doi.org/10.22033/ESGF/CMIP6.6674)
[98] Weiners K-H *et al* 2019e MPI-M MPI-ESM1.2-LR model output prepared for CMIP6 CMIP piControl Version 20190710 *Earth System Grid Federation* (https://doi.org/10.22033/ESGF/CMIP6.6675)
[99] Yukimoto S *et al* 2019e MRI MRI-ESM2.0 model output prepared for CMIP6 CMIP piControl Version 20191224 *Earth System Grid Federation* (https://doi.org/10.22033/ESGF/CMIP6.6900)
[100] Seland O *et al* 2019e NCC NorESM2-LM model output prepared for CMIP6 CMIP piControl Version 20210118 *Earth System Grid Federation* (https://doi.org/10.22033/ESGF/CMIP6.8217)
[101] Bentsen M *et al* 2019e NCC NorESM2-MM model prepared for CMIP6 CMIP piControl Version 20191108 *Earth System Grid Federation* (https://doi.org/10.22033/ESGF/CMIP6.8221)
[102] Tang Y, Rumbold S, Ellis R, Kelley D, Mulcahy J, Sellar A, Walton J and Jones C 2019b MOHC UKESM1.0-LL model output prepared for CMIP6 CMIP piControl Version 20200828 *Earth System Grid Federation* (https://doi.org/10.22033/ESGF/CMIP6.6298)
[103] O'Neill B C *et al* 2016 The scenario model intercomparison project (ScenarioMIP) for CMIP6 *Geosci. Model Dev.* **9** 3461–82
[104] Lyu K, Zhang X and Church J A 2020 Regional dynamic sea level simulated in the CMIP5 and CMIP6 models: mean biases, future projections, and their linkages *J. Clim.* **33** 6377–98
[105] Bouttes N, Gregory J M, Kuhlbrodt T and Smith R S 2014 The drivers of projected North Atlantic sea level change *Clim. Dyn.* **43** 1531–44
[106] Landerer F W, Jungclaus J H and Marotzke J 2007 Regional dynamic and steric sea level change in response to the IPCC-A1B scenario *J. Phys. Oceanogr.* **37** 296–312
[107] Megann A, Blaker A, Josey S, New A and Sinha B 2021 Mechanisms for late 20th and early 21st century decadal AMOC variability *J. Geophys. Res.* **126** e2021JC017865
[108] Huthnance J M, Coelho H, Griffiths C R, Knight P J, Rees A P, Sinha B, Vangriesheim A, White M and Chatwin P G 2001 Physical structures, advection and mixing in the region of Goban Spur *Deep-Sea Res.* II **48** 2979–3021
[109] Environment Agency 2019 LIDAR Composite DTM 2019–10m *Contains Public Sector Information Licensed Under the Open Government Licence v3.0* (available at: https://environment.data.gov.uk/dataset/f46accdf-0aed-47d0-8673-21789ed35afa) (Accessed July 2022)
[110] Marine Management Organisation, UK Government Water—tides and currents (available at: https://assets.publishing.service.gov.uk/government/uploads/system/uploads/attachment_data/file/535165/SA_Report_cards_Water.pdf) (Accessed July 2022)
[111] Spencer T, Brooks S M, Evans B R, Tempest J A and Möller I 2015 Southern North Sea storm surge event of 5 December 2013: water levels, waves and coastal impacts *Earth-Sci. Rev.* **146** 120–45
[112] Jevrejeva S, Jackson L P, Riva R E M, Grinsted A and Moore J C 2016 Coastal sea level rise with warming above 2 °C *Proc. Natl Acad. Sci. USA* **113** 13342–7
[113] IPCC 2021 Summary for policymakers *Climate Change 2021: The Physical Science Basis. Contribution of Working Group 1 to the Sixth Assessment Report of the Intergovernmental Panel on Climate Change V* (Cambridge : Cambridge University Press) pp 3–32
[114] Vitousek S, Barnard P L, Fletcher C H, Frazer N, Erikson L and Storlazzi C D 2017 Doubling of coastal flooding frequency within decades due to sea-level rise *Sci. Rep.* **7** 1399
[115] IPCC 2019 *Summary for Policymakers. In: IPCC Special Report on the Ocean and Croysphere in a Changing Climate* ed Pörtner H-O, Okem A, Petzold J, Rama B and Weyer N M (Cambridge: Cambridge University Press) pp 3–35
[116] Feser F, Barcikowska M, Krueger O, Schenk F, Weisse R and Xia L 2015 Storminess over the North Atlantic and northwestern Europe—A review *Q. J. R. Meteorol. Soc.* **141** 350–82
[117] Lewis M, Horsburgh K, Bates P and Smith R 2011 Quantifying the uncertainty in future coastal flood risk estimates for the U.K *J. Coast. Res.* **27** 870–81